Scanning Electron Microscopy

Volume 1982
Number 1 *1982*

Article 2

1982

Inelastic Scattering of Electrons in Solids

C. J. Powell
National Bureau of Standards

Electron Beam Interactions With Solids (Pp. 19-31)
SEM, Inc., AMF O'Hare (Chicago), IL 60666, U.S.A.

INELASTIC SCATTERING OF ELECTRONS IN SOLIDS*

C.J. POWELL
Surface Science Division, National Bureau of Standards
Washington, DC 20234
Tel. 301-921-2188

ABSTRACT

The principal mechanisms and available data for the inelastic scattering of electrons in solids are reviewed. The processes relevant for electron-probe microanalysis, electron energy-loss spectroscopy, Auger-electron spectroscopy, and x-ray photoelectron spectroscopy are described and examples of relevant electron energy-loss data are shown. The discussion is based on the dielectric description of inelastic scattering and treats processes important in the excitation of both core electrons and valence electrons. Information is given on the cross sections for excitations of valence electrons, cross sections for ionization of core levels, inelastic mean free paths of Auger electrons and photoelectrons in solids, and radiation damage.

Keywords: Inelastic electron scattering, inner-shell ionization cross section, inelastic mean free path, Auger-electron spectroscopy, electron energy-loss spectroscopy, electron-probe microanalysis, x-ray photoelectron spectroscopy, and radiation damage.

1. INTRODUCTION

Electrons incident on a solid or generated internally within a solid can be scattered elastically (with a change of momentum but without change of energy) or inelastically (with a change of energy). This article reviews the principal mechanisms and available data for the inelastic scattering of electrons by solids. Emphasis is placed on the processes relevant in microanalysis by electron-probe x-ray analysis and electron energy-loss spectroscopy (EELS), surface analysis by Auger-electron spectroscopy (AES) and x-ray photoelectron spectroscopy (XPS) and, to a lesser extent, radiation damage.

A summary of the relevant theory is given in Section 2. Sources of experimental dielectric data are identified and discussed in Section 3. The theory and the dielectric data are applied in Section 4 to several types of measurements of current interest. Attention is given to the physical processes affecting spectral shapes and cross sections in measurements of core-electron energy-loss spectra. The Bethe formula for inner-shell ionization is compared with experimental cross-section data and values of the "effective" Bethe parameters are given. A brief discussion is also given of various formulas that have been utilized for the variation of inner-shell ionization cross sections as a function of electron energy. The status of measurements and calculations of the inelastic mean free path for low-energy (50-2000 eV) electrons in solids is described and some results of new calculations of the dependence of mean free path on energy are presented. Finally, some brief remarks are given on radiation damage with particular reference to molecular dissociation caused by Auger transitions in compounds.

2. THEORY

The theory of inelastic scattering of electrons by solids has been summarized recently by Schnatterly (1979) and Raether (1980). A summary is given here of those aspects of the theory that are useful for the applications to be discussed in Section 4.

Inelastic electron scattering in solids can be described in terms of a complex dielectric constant $\epsilon(\omega,q)$ dependent on frequency ω and momentum-transfer q. For $q=0$, the dielectric constant is related to the familiar optical constants, the refractive index n and the extinction coefficient k, by

LIST OF SYMBOLS

A = Parameter in Eq. 18
B = Parameter in Eq. 18
$b_{n\ell}$ = Parameter in Bethe theory (Eq. 15)
c = Velocity of light
c_n = Parameter in Bethe theory (Eq. 13)
$c_{n\ell}$ = Parameter in Bethe theory (Eq. 15)
$c(E)$ = Parameter in Bethe theory (Eq. 14)
e = Electron charge
E = Energy loss
E_n = Particular energy loss
E_0 = Incident electron energy
$E_{n\ell}$ = Binding energy of electrons in $n\ell$-shell
f = Oscillator strength
$f_n(q)$ = Generalized oscillator strength
$\hbar$ = Planck's constant divided by 2π
k = Extinction coefficient
m = Electron mass
n = Refractive index
$n_{eff}(E)$ = "Effective" number of electrons per atom contributing to energy losses from 0 to E
N = Density of atoms
P = Momentum of incident electrons
q = Momentum transfer
q_{min} = Minimum momentum transfer
q_{max} = Maximum momentum transfer
$U_{n\ell}$ = $E_0/E_{n\ell}$
v = Electron velocity
Z = Atomic number
$Z_{n\ell}$ = Number of electrons in shell with principal quantum number n and angular momentum quantum number ℓ
ϵ = Complex dielectric constant
θ = Scattering angle
θ_E = $E/2E_0$
λ = Inelastic mean free path
μ_m = X-ray mass absorption coefficient
π = 3.14159
ϱ = Density
σ = Inelastic scattering cross section
$\sigma_{n\ell}$ = Ionization cross section for $n\ell$-shell
σ_T = Total inelastic scattering cross section
ω = Frequency
Ω_p = Plasma frequency

$$\epsilon(\omega,0) = (n + ik)^2 = \epsilon_1 + i\epsilon_2 \qquad 1a$$

$$\epsilon_1 = n^2 - k^2 \qquad 1b$$

$$\epsilon_2 = 2nk = \varrho c \mu_m/\omega \qquad 1c$$

In Eq. 1c, ϱ is the density of the solid, c is the velocity of light, and μ_m is the x-ray mass absorption coefficient.

The differential inelastic scattering cross section, per atom or molecule, for energy loss $E = \hbar\omega$ and momentum transfer q in an infinite medium is

$$\frac{d^2\sigma}{d\omega dq} = \frac{2e^2}{\pi N\hbar v^2} \mathrm{Im}\left[\frac{-1}{\epsilon(\omega,q)}\right]\frac{1}{q} \qquad 2$$

where N is the density of atoms, e is the electronic charge, $\hbar$ is Planck's constant divided by 2π, and v is the velocity of the incident electrons. For small scattering angles, $q \approx P(\theta^2 + \theta_E^2)^{1/2}$, P is the momentum of the incident electrons, θ is the scattering angle, $\theta_E = E/2E_0$, and E_0 is the incident electron energy. The relation given between q, P, θ, and θ_E is approximate although the approximation is very good in the context of the discussion in this paper. For Eq. 2 to be valid, it has been assumed that E_0 is much greater than E. It has also been assumed that $E \lesssim 50$ keV so that relativistic corrections [Inokuti (1971)] are not needed. Equation 2 can be extended to materials with crystalline anisotropies [Raether (1980)] but this complication will be ignored here. Finally, we do not consider modifications to Eq. 2 associated with the excitation of surface plasmons as these are not significant for most of the applications to be discussed.

The term

$$\mathrm{Im}\left(\frac{-1}{\epsilon}\right) = \frac{\epsilon_2}{\epsilon_1^2 + \epsilon_2^2} \qquad 3$$

in Eq. 2 is known as the energy loss function. The denominator in Eq. 3 is responsible for the differences that can occur between electron energy-loss spectra and optical absorption spectra (which are proportional to ϵ_2). For electron energy losses less than about 100 eV (i.e., losses predominantly due to valence-electron excitations), $\epsilon_1^2 + \epsilon_2^2$ is usually appreciably different from unity and there is a large difference between energy-loss and optical-absorption spectra. For energy losses greater than about 100 eV (i.e., losses predominantly due to core-electron excitations), $\epsilon_1 \approx 1$, $\epsilon_2 \ll 1$, so that $\mathrm{Im}(-1/\epsilon) \approx \epsilon_2$. Thus, electron energy-loss spectra are similar to x-ray absorption spectra.

Maxima occur in the energy loss function when

$$(\epsilon_1^2 - \epsilon_2^2)(d\epsilon_2/d\omega) - 2\epsilon_1\epsilon_2(d\epsilon_1/d\omega) = 0 \qquad 4$$

and $d^2[\mathrm{Im}(-1/\epsilon)]/d\omega^2$ is negative. Maxima in $\mathrm{Im}(-1/\epsilon)$ then occur *near* frequencies for which:

(a) there are maxima in ϵ_2 (excitation of interband transitions); or

(b) $\epsilon_1 = 0$, $\epsilon_2 \approx 0$ (excitation of volume plasmons).

Model calculations show how small changes in the position and strength of interband transitions affect the position and strength of maxima in the energy-loss function (Powell (1969)).

It is convenient to define the differential oscillator strength

$$\frac{df}{d\omega} = \frac{2\omega \mathrm{Im}[-1/\epsilon(\omega,q)]}{\pi\Omega_p^2} \qquad 5$$

where $\Omega_p = (4\pi Ne^2/m)^{1/2}$ and m is the electron mass. 6

The Thomas-Reiche-Kuhn sum rule is

$$\int_0^\infty (df/d\omega)\, d\omega = Z \qquad 7$$

where Z is the atomic number. The "effective" number of electrons per atom contributing to energy losses from 0 to E $= \hbar\omega$ is

$$n_{eff}(E) = \int_0^E (df/d\omega')\, d\omega' \qquad 8$$

Equations 2, 5 and 6 can be combined to give

$$\frac{d^2\sigma}{d\omega dq} = \frac{4\pi e^4}{mv^2} \cdot \frac{1}{q} \cdot \frac{1}{\hbar\omega} \cdot \frac{df}{d\omega} \qquad 9$$

For a relatively narrow energy-loss peak

$$\int \frac{1}{\hbar\omega} \cdot \frac{df}{d\omega} \cdot d\omega \approx \frac{1}{\hbar\omega_n} \int \frac{df}{d\omega} \cdot d\omega = \frac{f_n(q)}{E_n} \qquad 10$$

where an integration has been performed over a region of the differential oscillator strength appropriate for an energy loss centered at $E_n = \hbar\omega_n$.

Equation 9 becomes

$$\frac{d\sigma}{dq} \approx \frac{4\pi e^4}{mv^2} \cdot \frac{1}{E_n} \cdot \frac{f_n(q)}{q} \qquad 11$$

where $f_n(q)$ is the generalized oscillator strength for the energy loss E_n. Equation 11 is identical to the differential cross section derived by Bethe (1930) to describe the inelastic scattering of electrons by atoms.

The determination of either a total or a differential cross section for a loss E_n requires knowledge of the function $f_n(q)$, either from theory or experiment. Calculations of $f_n(q)$ for inner-shell excitations in atoms have been reported recently by Leapman *et al.* (1980) and by Inokuti and Manson (1983). We will assume for the moment that $f_n(q)$ is slowly varying in the region of small q where the differential cross section is largest. Thus,

$$f_n(q) \approx f_n(q_{min}) \approx f_n(0) \qquad 12$$

where q_{min} is the minimum momentum transfer corresponding to $\theta = 0$ and $f_n(0)$ is the optical oscillator strength. Equation 11 can now be integrated from $q_{min} = E_n/v$ to an "effective" upper limit $q_{max} = (mc_nE_n/2)^{1/2}$ where c_n is a constant, expected [Bethe (1930)] to be approximately 4, to yield

$$\sigma_n \approx \frac{2\pi e^4}{mv^2} \cdot \frac{f_n(0)}{E_n} \ln\left[\frac{c_n mv^2}{2E_n}\right] \qquad 13$$

Similarly, the differential cross section for energy loss E is

$$\frac{d\sigma}{dE} \approx \frac{2\pi e^4}{mv^2} \cdot \frac{1}{E} \cdot \frac{df}{dE} \cdot \ln\left[\frac{c(E)mv^2}{2E}\right] \qquad 14$$

where df/dE is the differential oscillator strength for q = 0 and c(E) is a function of E.

Bethe (1930) has expressed the total cross section per atom or molecule for ionization of the $n\ell$ shell (containing $Z_{n\ell}$ electrons with binding energy $E_{n\ell}$) in the form

$$\sigma_{nl} = \frac{2\pi e^4}{mv^2} \cdot \frac{Z_{nl} b_{nl}}{E_{nl}} \ln\left[\frac{c_{nl}E_0}{E_{nl}}\right] \qquad 15$$

Comparison of Eqs. 14 and 15 indicates that

$$b_{nl} = \frac{E_{nl}}{Z_{nl}\ln(c_{nl}E_0/E_{nl})} \int_{E_{nl}}^{E_{max}} \frac{1}{E} \frac{df}{dE} \ln\left[\frac{c(E)\,E_0}{E}\right] dE$$

$$\approx \frac{E_{nl}}{Z_{nl}} \int_{E_{nl}}^{E_{max}} \frac{1}{E} \frac{df}{dE}\, dE \qquad 16$$

where E_{max} is large compared to E_{nl} and assumed for the moment to be less than the binding energy of the next most tightly bound shell. It is convenient to rewrite Eq. 15 in the form

$$\sigma_{nl} E_{nl}^2 = \pi e^4 Z_{nl} b_{nl} \ln(c_{nl} U_{nl})/U_{nl} \qquad 17$$

where $U_{nl} = E_0/E_{nl}$. Equation 17 provides a convenient means for comparing values of $\sigma_{nl}E_{nl}^2$ for different elements in terms of the dimensionless variable U_{nl}. Furthermore, the linearity of a so-called Fano plot of $\sigma_{nl}E_{nl}^2\, U_{nl}/\pi e^4\, Z_{nl}$ versus $\ln U_{nl}$ for a given element indicates the range of U_{nl} that the Bethe equation (Eq. 15) is valid and provides a convenient means of determining the parameters b_{nl} and c_{nl}.

The major questions concerning the applicability of the preceding theory to the experimental situations of interest are:

(a) By how much should the incident energy E_0 exceed the threshold energy $E_{n\ell}$ for Eqs. 13-15 to give accurate cross sections?

(b) What are the optimum values of the parameters $b_{n\ell}$ and $c_{n\ell}$ in Eq. 15 and can they be obtained from integrations of differential oscillator strength, either measured or calculated, over energy transfer (Eq. 16) and momentum transfer (Eqs. 11-13), respectively?

(c) Are there other cross-section formulations (e.g., quantum-mechanical calculations for specific atoms or semi-empirical formulas) that provide a better means than the above Bethe equations for predicting inelastic scattering cross sections?

These questions will be addressed later in this article.

3. EXPERIMENTAL DIELECTRIC DATA

As cross sections for inelastic electron scattering in solids are directly proportional to the energy-loss function (Eq. 2),

it is useful to indicate sources of experimental dielectric data and to examine certain trends. Measurements of Im $[-1/\epsilon(\omega,q)]$ have been reviewed recently by Schnatterly (1979) and by Raether (1980). The majority of the measurements are of energy loss spectra, obtained by transmission through thin specimen films for $\theta=0$, from which values of Im $[-1/\epsilon(\omega, q_{min})] \approx$ Im $[-1/\epsilon(\omega)]$ have been obtained. These measurements have been compared with values of Im $[-1/\epsilon(\omega)]$ determined by optical methods at visible, ultraviolet, and x-ray frequencies with generally adequate agreement.

The growing availability of sources of synchroton radiation has led to increasing amounts of optical absorption data in the ultraviolet and x-ray spectral regions. Sources of data are Hagemann *et al.* (1974), Haelbich *et al.* (1977), Winick and Doniach (1980), and Weaver *et al.* (1981). The book edited by Winick and Doniach (1980) also contains reviews of the various physical processes important in photoabsorption.

Figures 1-3 are plots of Im $[-1/\epsilon(\omega,0)]$ for Al, Cu, and Au from the compilation of Hagemann *et al.* (1974). The plot for Al in Fig. 1 shows a strong maximum at E = 15 eV that has been identified as being due to volume plasmon excitation and other structure for E > 72 eV associated with excitations of L_{23}-shell electrons (see also Section 4.1). By contrast, the plots of Im $[-1/\epsilon(\omega,0)]$ for Cu and Au show a broader distribution of the energy loss function than for Al in the region of valence-electron excitations with E < 50 eV, and the structures associated with the onset of inner-shell excitations (expected at the M_3 threshold at 75 eV in Cu and at the N_7, N_5, and N_3 thresholds in Au at 84 eV, 335 eV, and 546 eV, respectively) are not prominent. The lack of prominence of the inner-shell thresholds in Cu and Au is due in large part to the delayed onset of oscillator strength associated with the "centrifugal barrier" in the potential [Fano and Cooper (1968), Leapman *et al.* (1980)]. Comparison of the Im $[-1/\epsilon(\omega,0)]$ data for Cu and Au with the corresponding plots of $\epsilon_1(\omega)$ and $\epsilon_2(\omega)$ [Hageman, *et al.* (1974)] indicates that the structure in the energy loss function for these two metals is largely associated with the excitation of interband transitions and a damped volume plasmon (cf. Eq. 4).

It is clear from Figs. 1-3 (and similar data for other materials) that the most probable energy loss is typically 5-40 eV. The cross section for inelastic scattering (Eq. 2) is therefore largest for excitations of valence electrons.

Figures 4-6 are plots of $n_{eff}(E)$ (Eq. 8) for Al, Cu, and Au from Hagemann *et al.* (1974). The plot of $n_{eff}(E)$ for Al in Fig. 4 indicates that $n_{eff}(E)$ "saturates" at about 3, the number of valence electrons, for E = 70 eV, just below the threshold for L-shell excitation. The integration from 70 eV to 1500 eV indicates an effective number of about 9 electrons, slightly more than the number of electrons in the L shell; note the $n_{eff}(E)$ does not "saturate" again until E exceeds 1000 eV. Shiles *et al.* (1980) have made a further analysis of optical data for Al and have shown the existence of some inaccuracies in the optical data as well as some inconsistencies in the analysis of Hagemann *et al.* (1974). The trends shown in Fig. 4 are preserved in the new analysis but $n_{eff}(E)$ now saturates at the expected value of 13 for $E > 10^4$ eV.

The plots of $n_{eff}(E)$ for Cu and Au in Figs. 5 and 6 are qualitatively different from that for Al. For Cu and Au, there is not an obvious saturation of the oscillator strength for the excitations for each shell. Instead, the oscillator-strength distribution for one shell often overlaps with that for another shell. In cases such as these, it is not possible to derive a total oscillator strength for a given shell.

Information on the q-dependence of Im $[-1/\epsilon(\omega,q)]$ is rather sparse. Measurements have been reported of the q-dependence of energy-loss spectra associated with valence-electron excitations [Raether (1980), Schnatterly (1979)] for a number of materials; most measurements pertain to the dispersion of volume plasmons with varying momentum transfer. A few measurements have been made of inner-shell electron energy-loss spectra [Schnatterly (1979)] as a function of momentum transfer although the emphasis of this work has been on the spectrum shape close to the core-level threshold. Measurements of the q-dependence of Im $[-1/\epsilon(\omega,q)]$ are, in general, difficult as the signal of interest can be overwhelmed by electrons which have been inelastically scattered through small angles (where the differential cross section is large) and elastically scattered to the angle of observation.

4. APPLICATIONS

4.1 Electron Energy-Loss Spectroscopy

We consider now measurements of the energy-loss spectra of high-energy ($\approx$ 50 keV) electrons transmitted through thin ($\approx$ 100 nm) specimen films with a zero or small scattering angle. The features of interest here are those associated with the excitation of inner-shell electrons ($50 \leq E \leq 2000$ eV) which are useful for microanalysis.

Figures 7 and 8 illustrate EELS data for Al and Al_2O_3 [Swanson and Powell (1968)]. Figure 7 shows the energy-loss spectrum of 20 keV electrons transmitted through a 300 Å Al film. The strong loss peak at E $\approx$ 15 eV is due to volume plasmon excitation (cf. Fig. 1) and the features with diminishing intensity at 30, 45, and 60 eV energy loss are due to multiple plasmon excitations. The plasmon features appear on an exponentially decreasing background that has intensity contributions from additional excitation processes of large energy loss in Al (Fig. 1) and to inelastic scattering by the oxide layers on the specimen surface. The shape of this background is also influenced by variation of the effective angular resolution with E; the spectrometer had a fixed angular acceptance and therefore accepted a decreasing fraction of the total angular distribution of inelastically scattered electrons with increasing E. Also seen in Fig. 7 is an increase in energy-loss intensity at E $\approx$ 72 eV associated with the excitation of L-shell electrons. This region of the energy-loss spectrum is shown in greater detail in Fig. 8(a) together with similar spectra for $\gamma - Al_2O_3$ and anodized Al_2O_3 in Figs. 8(b) and 8(c). The spectra in Fig. 8 indicate that there is a small chemical shift in the Al L-shell excitation threshold from the metal to the oxide, that the near-edge structures in the different forms of Al_2O_3 are different, that a background (the long-dashed line) can be found by extrapolation from the region of valence-electron excitation, and that a correction can be made (the short-dashed line) for combined L-shell and plasmon excitations.

We will assume for the moment that E_0 is sufficiently high, $50 \leq E_0 \leq 2000$ eV, and that the electron scattering angles are sufficiently small so that q_{min} is "small" and Im $[-1/\epsilon(\omega,0)] \approx \epsilon_2$ (Eq. 3). Electron energy-loss spectra measured under these conditions should therefore correspond closely to x-ray absorption data. We consider now a number of phenomena that can modify structure or give rise to new structure in EELS data, particularly in the vicinity of the core-electron

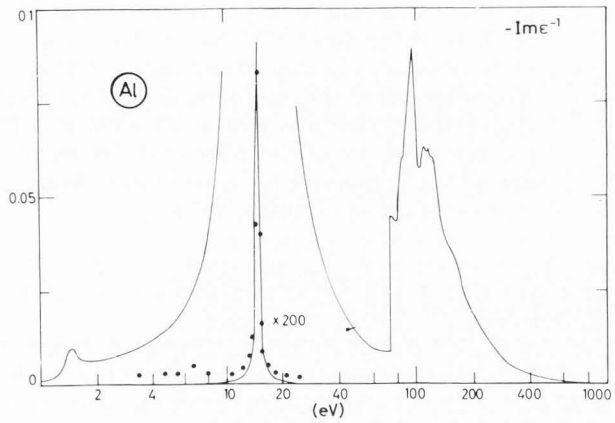

Fig. 1. Plot of the energy loss function for Al from optical data; the solid points are measurements from electron energy-loss spectra [Hagemann *et al.* (1974)].

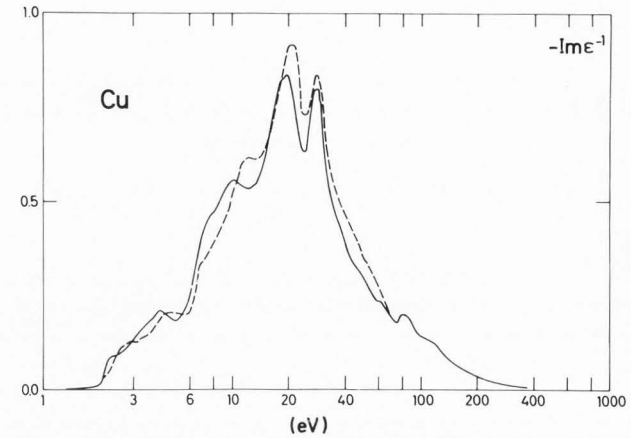

Fig. 2. Plot of the energy loss function for Cu from optical data (solid line): the dashed line gives results from electron energy-loss spectra [Hagemann *et al.* (1974)].

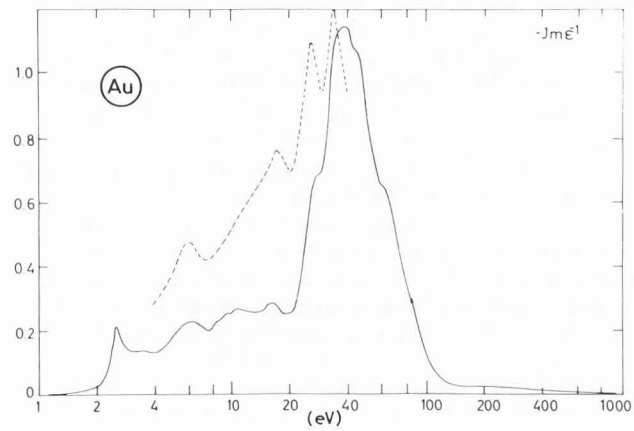

Fig. 3. Plot of the energy loss function for Au from optical data (solid line); the dashed line gives results from electron energy-loss measurements [Hagemann *et al.* (1974].

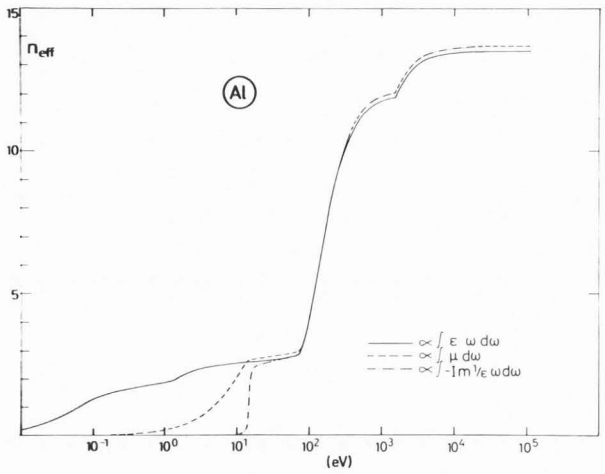

Fig. 4. Plot of $n_{eff}(E)$ for Al (Eq. 8), dot-dashed line; the other curves are results of integrations of other optical data [Hagemann *et al.* (1974)]. Revised values of $n_{eff}(E)$ for Al have been published recently by Shiles *et al.* (1980) (see text).

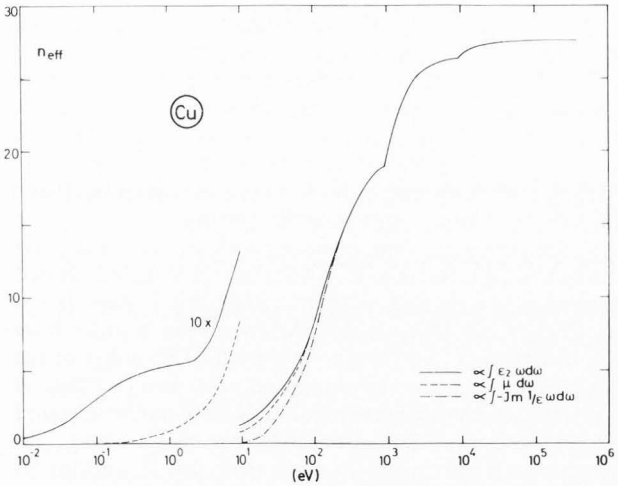

Fig. 5. Plot of $n_{eff}(E)$ for Cu, dot-dashed line [Hagemann *et al.* (1974); see also caption to Fig. 4.

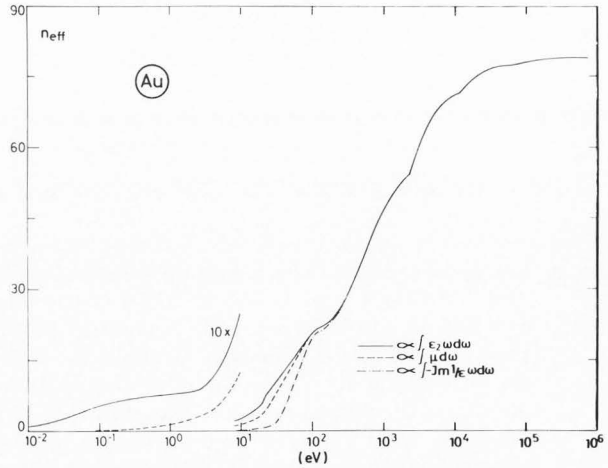

Fig. 6. Plot of $n_{eff}(E)$ for Au, dot-dashed line [Hagemann *et al.* (1974)]; see also caption to Fig. 4.

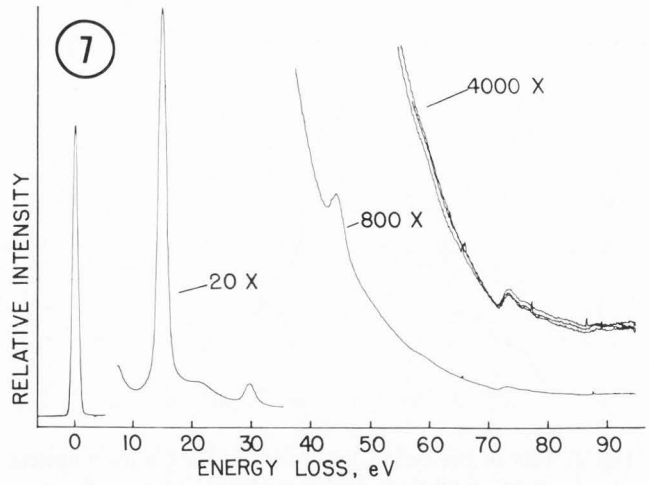

Fig. 7. Energy-loss spectrum of 8.2 $\mu g/cm^2$ (300 Å) Al films for $E_0 = 20$ keV and $\theta \approx 0$. The angular acceptance of the analyzer was a cone of half-angle ≈ 0.25 mrad and the angular distribution of the incident beam was approximately Gaussian with a full width at half-maximum intensity of about 1.6 mrad. The relative-gain setting is indicated for each intensity change of scale [Swanson and Powell (1968)].

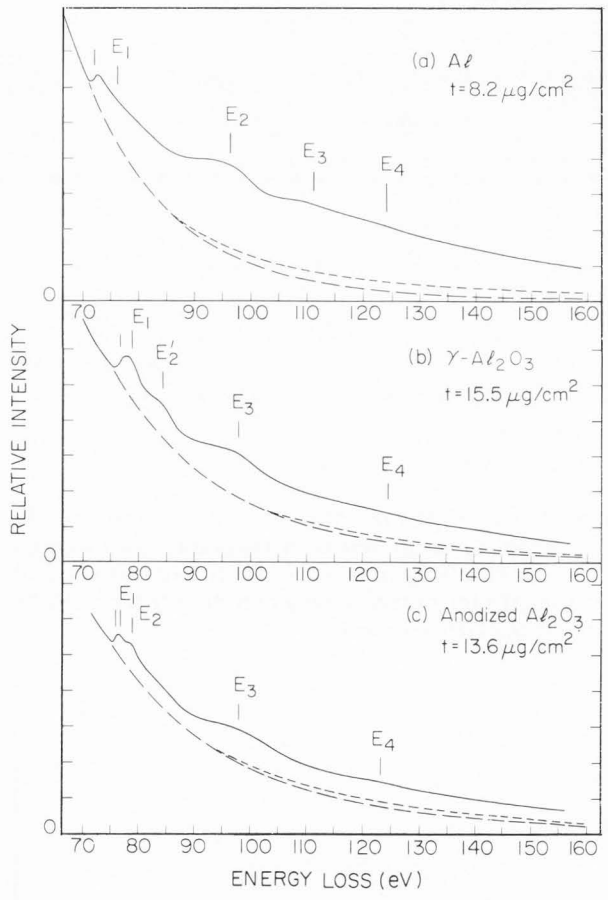

Fig. 8. Energy-loss spectra in the region corresponding to L-shell excitation for (a) Al, (b) $\gamma - Al_2O_3$ prepared by oxidizing an Al film in air, and (c) anodized Al_2O_3. The backgrounds determined by extrapolation of the energy-loss intensities below the absorption edges are shown as long-dashed lines and the additional contributions from electrons exciting both a volume plasmon and an L-shell electron are shown as short-dashed lines [Swanson and Powell (1968)].

thresholds that are useful for microanalysis. These phenomena need to be considered for both qualitative and quantitative analyses.

(1) Chemical Shifts of Thresholds. The same element in different chemical environments can be expected to show different core-electron threshold energies in EELS data. These shifts, often of about 1-2 eV, correspond to the chemical shifts observed in x-ray photoelectron spectroscopy [Siegbahn *et al.* (1974), Wagner *et al.* (1979)] and can provide useful information about the chemical state of a particular element.

(2) Edge Singularities. The detailed shape of an x-ray absorption "edge" within ~1 eV of the threshold energy is influenced by the excitation of electron-hole pairs in response to the creation of the core hole in a particular shell [Schnatterly (1979), Citrin *et al.* (1979)]. The specific edge shapes that can occur are of little significance in EELS experiments with current energy resolutions.

(3) Near-Edge Structure. Structure within about 50 eV of a core threshold is often observed (Fig. 8). This structure is due in part to atomic contributions to df/dE for a particular element [Fano and Cooper (1968), Leapman *et al.* (1980)] and in part to the details of the solid-state band structure. The absorption spectra of an element in different chemical environments can be expected to have structure at different energies (Fig. 8). This structure can also be useful for giving chemical-state information.

(4) EXAFS. The extended x-ray absorption fine structure, broad maxima extending several hundred electronvolts above an absorption edge, can be analyzed to give structural information of atoms about an absorption site [Teo and Joy (1981)].

(5) Delayed Onsets. For some core levels, the photoabsorption will increase sharply near the core threshold energy and then decrease while for others the increase in photoabsorption at the threshold will be extremely small. In the latter cases, the photoabsorption will increase and reach a maximum about 20-200 eV above the threshold energy due to a strong centrifugal barrier in the absorption potential [Fano and Cooper (1968), Leapman *et al.* (1980)].

(6) Fano Profiles. The shape of an absorption "edge" may be modified appreciably by interfering excitation channels which have discrete and continuum intermediate states [Fano and Cooper (1968)]. Asymmetric absorption profiles have been observed in photoabsorption and EELS studies of the M_{23} excitations in the transition and noble metals [Dietz *et al.* (1980)]. A striking manifestation of the Fano interference effect is the contrast in the threshold shapes of the Ni L_3 absorption spectrum, which shows a peak due to unfilled 3d states [Leapman and Grunes (1980)] and the Ni M_{23} absorption spectrum, which shows an asymmetrical step [Jach and Powell (1981)].

(7) Multiple Scattering. Additional intensity (and structure) can appear in EELS data due to a combination of inner-shell excitation and valence-electron excitation (Fig. 8). Unless the specimen thickness is much less than the total inelastic mean free path for the particular incident energy, correction of measured EELS intensities (e.g., by deconvolution of the loss spectrum measured for small energy losses) will be needed.

(8) Satellites. The sudden creation of a core-electron vacancy will generally lead to excitation of the valence electrons, either of a single valence electron (thus creating a two-hole final state) or a large number of valence electrons (an intrinsic plasmon). Details of different "final-state" effects have been described by Gadzuk (1978) and Shirley (1978).

The measured energy-loss intensity distribution will depend on an integration of the differential scattering cross section (Eq. 9) appropriate to the angular acceptance of the particular spectrometer. Leapman *et al.* (1980) have pointed out that the measured intensity distributions for a collection angle of 0.1 rad can depart significantly (e.g., by up to about 30% for carbon K-shell excitation with E_0 = 80 keV) from the photoabsorption spectrum. The total intensity within, say, 50 eV of the core threshold will be given by an additional integration of Eq. 9 over energy transfer for the limits of particular interest. This total intensity, which is needed for quantitative microanalysis, will depend on the physical processes discussed above and the chemical environment of the particular atom. The extent to which these phenomena influence observed intensities has not been explored in sufficient detail to predict "sensitivity factors" or "correction factors" for a wide range of elements and materials.

It is clear now that the simple model of EELS data near a core-electron threshold consisting of a sharp jump in the loss intensity followed by an exponential decay is of limited validity. There is a need for more experimental EELS data and calculations of the generalized oscillator strength (Eqs. 5, 9 and 11) so that the significant processes in a range of materials can be identified.

4.2 Total Cross Sections for Inner-Shell Ionization

Consideration is given now to the total cross sections for ionization of inner-shell electrons by electron impact. Inner-shell vacancies can decay either by the emission of characteristic x-rays or of Auger electrons. The yield of x-rays or Auger electrons is *not* necessarily proportional to the vacancies produced by electron impact; internal redistribution of the inner-shell vacancies often occurs by Auger or Coster-Kronig processes [Bambynek *et al.* (1972)] prior to the x-ray or Auger-electron emission of interest. In practical electron-probe microanalysis (EPMA) and Auger-electron spectroscopy (AES), ionizations by back-scattered electrons have to be considered in addition to those that may be produced by the incident electron beam. The backscattered electrons (due to incident and secondary electrons that have been multiply scattered by a chain of elastic and inelastic events) also give rise to a background in AES on which the Auger-electron signal of interest appears. Total cross sections for both inner-shell ionization and for all types of inelastic scattering are needed to predict overall yields in EPMA and AES and the ratio of signal and background intensities in AES.

Total cross sections for inner-shell ionization can be computed from integration of the generalized oscillator strength (Eqs. 9 and 11). Inokuti (1971) has shown that total cross sections for inelastic scattering for atoms can be calculated from atomic properties.

Experimental inner-shell ionization cross-section data have been analyzed to test for consistency with the Bethe equation (Eq. 15) and to derive "effective" values of the parameters b_{nl} and c_{nl} (Powell 1976a, 1976b). Figure 9 is a plot of experimental values of $\sigma_K E_K^2$ versus U_K, as suggested by Eq. 17, for a number of elements. Most of the data appears to be close to a common curve and it therefore appears that b_K does not depend on Z to a significant extent. A similar plot of $\sigma_{L_{23}} E_{L_{23}}^2$ as a function of $U_{L_{23}}$ is shown in Fig. 10. These data indicate an increase of $b_{L_{23}}$ with Z.

Figures 11 and 12 are Fano plots for the experimental K-shell and L_{23}-shell cross-section data. The range of U_{nl} for which these plots are linear indicates directly where the Bethe cross-section equation can adequately describe the measured data. Linear regions are found typically in the range $4 \leq U_{nl} \leq 25$.

"Effective" values of the Bethe parameters b_{nl} and c_{nl} can be easily found by linear least-squares fits to the appropriate linear regions in Figs. 11 and 12. The results of these fits [Powell (1976a)] are summarized in Table 1. The values of b_K derived in this way were larger and the values of c_K smaller than those expected from calculated K-shell ionization cross sections. Values of b_K and also of $b_{L_{23}}$ were therefore calculated from x-ray absorption cross sections with the use of Eq. 16. The results of this calculation are shown in Table 2 from which it can be seen that the "optical" values of b_{nl} are lower than those found from ionization cross-section measurements. The reason for these differences can be understood from the fact that the differential oscillator strength is not concentrated in a narrow range of excitation energies near the threshold energy E_{nl}. It is clear from Figs. 1-6 that the differential oscillator strength is extended over a considerable range of excitation energies, often up to about 10 E_{nl} (particularly for materials that have delayed onsets in the absorption away from their threshold E_{nl}). It might then be expected that the incident energy might have to be large as, say, 30 E_{nl} for E_0 to be large compared to all significant excitation energies and for Eq. 15 to be valid with a value of b_{nl} consistent with x-ray absorption data (Eq. 16).

To test the validity of the above ideas, it was decided to set c_{nl} = 2.42 [a value originally recommended by Mott and Massey (1949)] and to compute b_{nl} as a function U_{nl} from the experimental cross-section data. Values of b_{nl} derived in this way are plotted in Fig. 13 and show the expected trends. For low U_{nl}, the value of b_{nl} is small because only a relatively small fraction of the differential oscillator strength is available for excitation. As U_{nl} is increased, more oscillator strength becomes available until, at a sufficiently large value of U_{nl}, all of the oscillator strength for the shell is available for excitation. The derived values of b_{nl} in Fig. 13 appear to saturate as expected for increasing U_{nl}. Also, the "saturation" values of b_K are now close to those expected from photoabsorption data (Table 2).

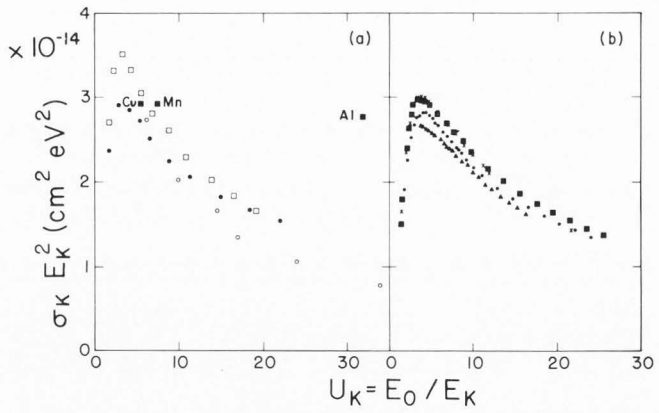

Fig. 9. Experimental value of $\sigma_K E_K^2$ as a function of U_K. (a) data for C (open circles), Al (open squares), and Ni (solid circles); the solid squares represent data for Al, Mn, and Cu by Fischer and Hoffman (1967). (b) data for C (triangles), Ne (crosses), N (squares), and O (circles) [Powell (1976a)].

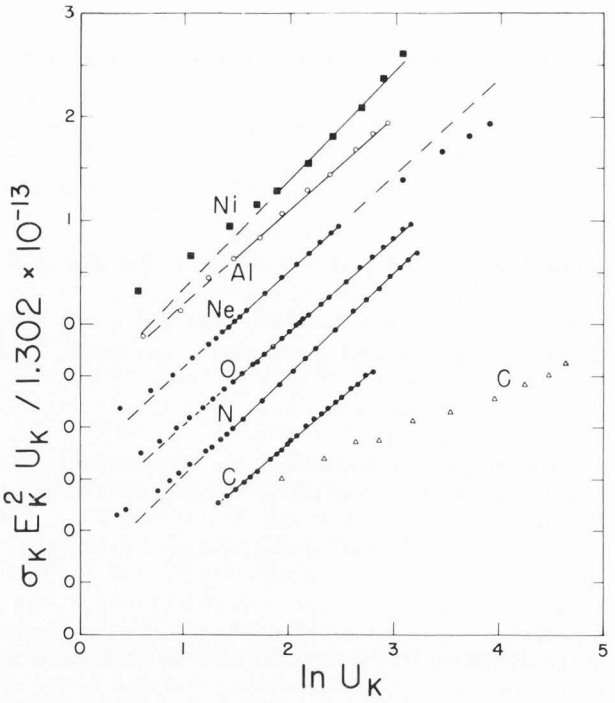

Fig. 11. Plot of experimental values of $\sigma_K E_K^2 U_K / 1.302 \times 10^{-13}$ versus ln U_K (a Fano plot based on Eq. 17.) Successive plots have been displaced vertically for clarity. The solid lines represent linear least-square fits for the range of U_K indicated in Table 1; the dashed lines are extrapolations. The derived Bethe parameters are also shown in Table 1 [Powell (1976a)].

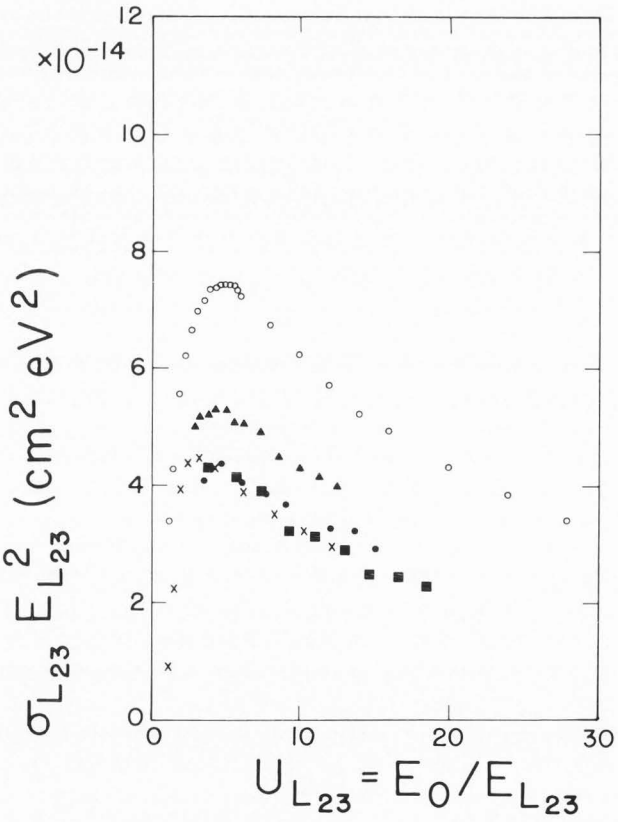

Fig. 10. Experimental value of $\sigma_{L_{23}} E_{L_{23}}^2$ as a function of $U_{L_{23}}$. Data shown is for P (squares), S (circles), Cl (triangles), and Ar (crosses and open circles) [Powell (1976a)].

Table 1. Effective values of the Bethe Parameters found from linear least-squares fits to the experimental cross-section data in Figs. 11 and 12 [Powell (1976a)].

Shell	Range of U_{nl}	Bethe Parameters
K-shell	$4 \leq U_K \leq 25$	$b_K \approx 0.9$
		$c_K \approx 0.65$
L_{23}-shell	$4 \leq U_{L_{23}} \leq 20$	$b_{L_{23}} \approx 0.6$-0.9
		$c_{L_{23}} \approx 0.6$

Table. 2 Values of the Bethe parameter b_{nl} found from x-ray absorption data with the use of Eq. 16 for the elements indicated (Powell 1976a)

Shell	Bethe Paramater b_{nl}
K-shell	$b_K = 0.55 \pm 0.05$ (Be, C, O, Ne)
L_{23}-shell	$b_{L_{23}} = 0.55 \pm 0.06$ (Al, Si, S, Ar)

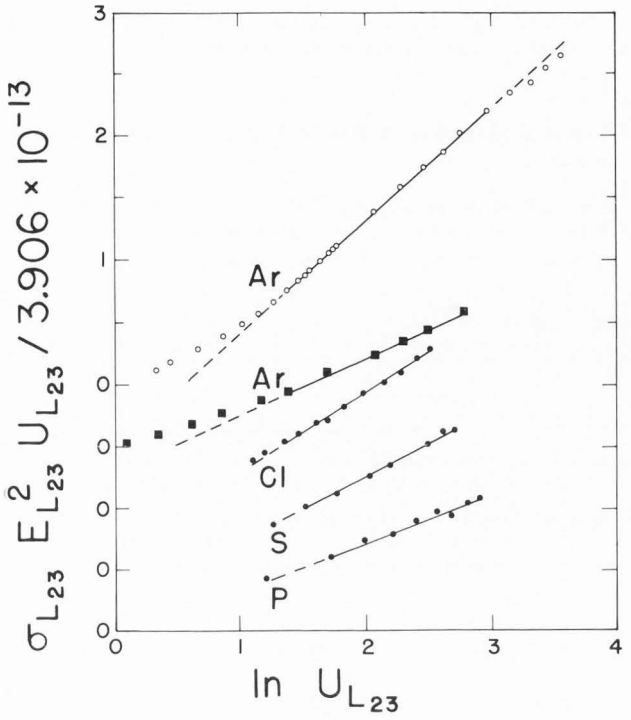

Fig. 12. Plot of experimental values of $\sigma_{L_{23}} E_{L_{23}}{}^2 U_{L_{23}} / 3.906 \times 10^{-13}$ versus ln $U_{L_{23}}$ (a Fano plot based on Eq. 17). See also caption to Fig. 11 [Powell (1976a)].

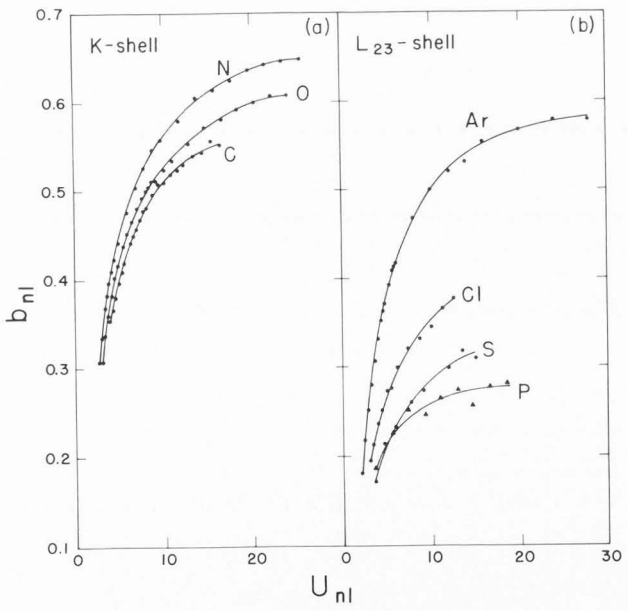

Fig. 13. Plot of the effective value of the Bethe parameter b_{nl} as a function of U_{nl} found by assuming c_{nl} = 2.42 in Eq. 15. The parameter b_{nl} was calculated from the experimental (a) K-shell and (b) L_{23}-shell cross-section data plotted in Figs. 9 and 10 [Powell (1976a)].

The value of c_{nl} may not, of course, be correct so the numerical values in Fig. 13 are of limited significance. It is also possible that c_{nl} could be a function of excitation energy (Eq. 16) and thus also of U_{nl}. Nevertheless, the trends in Fig. 13 appear qualitatively reasonable from the known distributions of differential oscillator strength. The derived values of $b_{L_{23}}$ in Fig. 13, however, are rather lower than those expected from photoabsorption data and there is thus an apparent inconsistency between the cross-section and photoabsorption data.

The preceding discussion indicates that the effective values of b_{nl} and c_{nl} in Table 1 should be regarded as empirical parameters useful only in the range of U_{nl} indicated. The fact that Fano plots of the type shown in Figs. 11 and 12 are linear establishes the utility of the Bethe equation as an empirical formula but does not guarantee accuracy over a larger range of U_{nl} and consistency with optical data. Further, Fano plots for other shells could be qualitatively different than those in Figs. 11 and 12 if the distributions of oscillator strength differ significantly (e.g., if there are large delayed onsets of absorption) from those for the elements considered here.

A large number of theoretical and empirical formulas have been proposed to describe inner-shell ionization cross sections (Powell 1976b). Figure 14 is a comparison of experimental cross-section data for K-shell ionization and results expected from a number of formulas. Fig. 14(a) is a plot of $\sigma_K E_K{}^2$ for C, Ne, N, and O (also given in Fig. 9) as a function of U_K. The solid line is a smooth curve drawn through the experimental points; the same curve has been drawn in the other panels to serve for comparison with other results. The dashed curve in Fig. 14(a) is the Bethe equation, Eq. 15, with $b_K = 0.9$ and $c_K = 0.65$, the empirical values for these parameters found from the Fano plots (Fig. 11) and shown in Table 1. The other panels (Figs. 14(b), (c), (d) show plots of $\sigma_K E_K{}^2$ from the formulas or calculations of Worthington and Tomlin (1956), Green and Cosslett (1961), Drawin (1963), Gryzinski (1965), Lotz (1970), McGuire (1971), Rudge and Schwartz (1966), and Kolbenstvedt (1967); details of the formulas and parameters are given in Powell (1976b). It can be seen that few of the formulas fit the experimental data particularly well. The formulas of Drawin (1963) and Lotz (1970), however, could fit the experimental curve if the amplitudes of the calculated cross section were increased by about 10% and 25%, respectively. These formulas would appear to be particularly useful for the threshold region ($1 < U_K < 4$).

It is clear that more measurements are needed of inner-shell ionization cross sections. We do not now have an adequate description of the variation of the cross sections as a function U_{nl} over a large range of U_{nl}. It would, of course, be desirable to have measurements of the generalized oscillator strength. Further measurements are needed of L-shell ionization cross sections to remove a discrepancy in current data. There are few measurements of M-shell and N-shell ionization cross sections. The known delayed onsets in photoabsorption are expected to modify the shape of the cross-section curve as a function of U_{nl} near threshold. Smith and Gallon (1974) have found delayed onsets in the cross-section for N_{67}-shell ionization in Au, Pb, and Bi; little

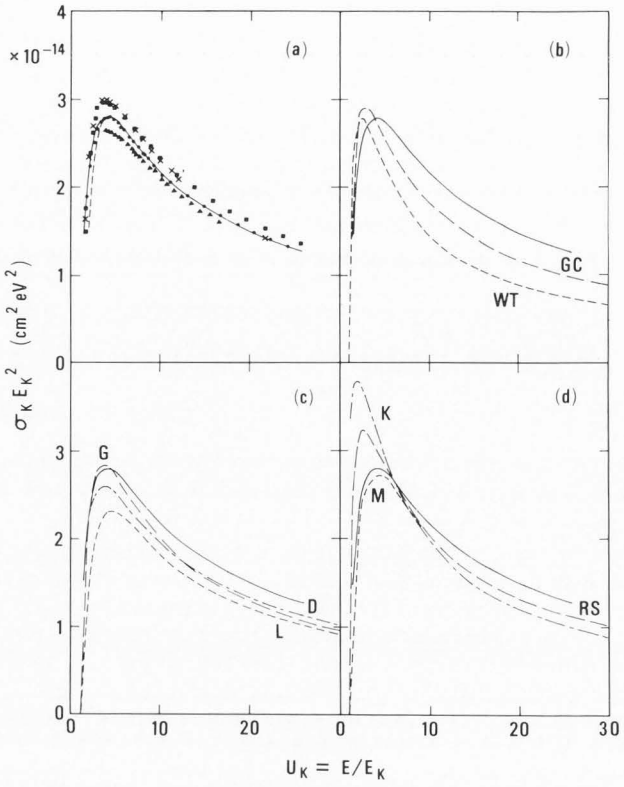

Fig. 14. Plot of $\sigma_K E_K^2$ against U_K. (a) Experimental values for C (triangles), neon (crosses), nitrogen (squares), and oxygen (circles) have been plotted from Fig. 9(b). The solid line in Figures 14(a), (b), (c), (d) is a smooth curve through the experimental points. The dashed curve is Eq. 17, the Bethe equation, with $b_K = 0.9$ and $c_K = 0.65$. The other panels are the results of specific cross-section calculations or suggested formulas. (b) The short-dashed curve (WT) is the Worthington and Tomlin (1956) equation and the long-dashed line (GC) is the Green and Cosslett (1961) equation. (c) the short-dashed line (L) is the Lotz (1970) equation, the long-dashed curve (G) is the result of Gryzinski (1965), and the dot-dashed curve (D) is the result of Drawin (1963). (d) the short-dashed curve (M) represents calculations of McGuire (1971) for Be, C, and O, the long-dashed line (RS) is the result of Rudge and Schwartz (1966), and the dot-dashed curve (K) is the result of Kolbenstvedt (1967) [Powell (1976b)].

Fig. 15. Calculation of the inelastic mean free path in elemental solids as a function of Z according to the results of Penn (1976). The values shown here are for $E_0 = 1000$ eV. The solid circles denote results for free-electron-like solids which are expected to be more accurate than the estimates shown as open circles for non-free-electron-like solids. For the former type of solids, volume plasmon excitation is the predominant inelastic mechanism while for the other solids interband transitions become important (Figs. 1-3) [Powell (1968)].

ionization was observed until $U_{N_{67}}$ reached 1.5-2.0. For such cases, formulas of the type plotted in Fig. 14 would have to be modified significantly.

4.3 Inelastic Mean Free Paths of Low-Energy Electrons in Solids

The inelastic mean free path of low-energy (50-2000 eV) electrons in solids is needed for quantitative surface analysis by AES and XPS. Absolute values of mean free paths are required in comparisons of intensities for an element in different chemical environments (i.e., a matrix correction) while relative values of mean free paths are needed in comparisons of the intensities from two or more elements in a single specimen material [Powell (1978)].

Seah and Dench (1979) have published a compilation of inelastic-mean-free-path data for a variety of materials. Accurate measurement of inelastic mean free paths is difficult, [Powell (1974)] and it is not surprising that there is considerable scatter in measurements from different laboratories. The fact that inelastic mean free paths can differ considerably from material to material (for a fixed electron energy) is clear from calculations such as those of Penn (1976). Figure 15 is a plot of the inelastic mean free paths for $E_0 = 1000$ eV as a function of Z [Powell (1978)]. Although there are a number of approximations in the calculated values, particularly for non-free-electron solids, it is clear from Fig. 15 that systematic variations of the inelastic mean free path in different materials are to be expected. Other calculations of the inelastic mean free path for a number of solids have been published recently by Szajman and Leckey (1981) and by Ashley and Tung (1982).

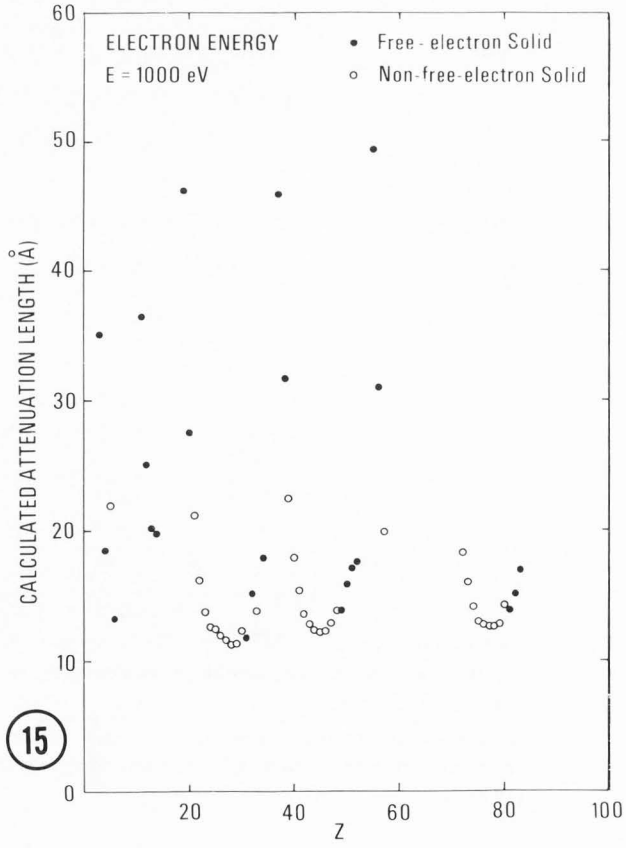

Seah and Dench (1979) proposed the following general relationship between the inelastic free path λ in a given material and the electron energy E_0:

$$\lambda = (A/E_0^2) + B E_0^{1/2} \quad 18$$

where A and B are material-dependent parameters. Wagner *et al.* (1980) have analyzed the dependence of λ on E_0 for a number of materials for which at least several measurements at different energies have been made in the same laboratory; it was believed that the variation of λ with E_0 could be established with reasonable accuracy even if the absolute values of λ could be in error. Wagner *et al.* (1980) suggested the more general relation:

$$\lambda = k E_0^m \quad 19$$

for $E_0 \gtrsim 300$ eV and derived values of the parameter m from experimental data. They found that m could be as high as 0.81 for Si and as low as 0.54 for Au and Al_2O_3. Szajman *et al.* (1981) have proposed that m = 0.75 while Ashley and Tung (1982) have found, in calculations of λ for a number of materials, that the exponent m could vary between 0.77 (for Al) and 0.69 (for Au).

The inelastic mean free path is related to the total inelastic scattering cross section σ_T by

$$\lambda = 1/N\sigma_T \quad 20$$

The total inelastic cross section can be calculated from an integration of Eq. 2 over all energy and momentum transfers appropriate for a particular "incident" electron energy E_0. Equations 15 and 16 can be generalized to give

$$\lambda = \frac{3.327\ E_0}{\int_0^{E_{max}} \mathrm{Im}\,[-1/\epsilon(E)]\ \ell n\ (c\ E_0/E)\,dE}\ \text{Å} \quad 21$$

where the energy E_0 has been expressed in electron volts and E_{max}, the upper limit for the integration, is less than E_0. The term c in Eq. 21 is analogous to c_{nl} in Eq. 15 and thus should depend, in general, on the momentum dependence of the energy-loss function. For the reasons discussed in Section 4.2, however, c can be regarded as an empirical parameter.

Equation 21 has been evaluated using the optical data of Hagemann *et al.* (1974) for a number of materials. Calculations have been made for electron energies between 300 and 2000 eV and these values have been fitted to Eq. 19 to derive a value for the exponent m. If c is set equal to 2.0 [a reasonable value based on Penn's (1976) calculations], the exponent m is found to range between 0.75 for Al and 0.69 for Au in close agreement with the results of Ashley and Tung (1982). If c is set equal to 0.65, the empirical value of c_{nl} found in analyses of K- and L_{23}-shell cross sections, the exponent m is found to range between 0.65 for Al and 0.55 for Au. While the "true" value of c is not known, it is apparent that the exponent m can depend on the nature of the distribution of oscillator strength for the energy-loss function (Figs. 1-3) and can thus be reasonably expected to vary in the range of $\approx 0.55 - 0.75$ for different materials.

4.4 Radiation Damage

The interaction of electrons with solids can lead to various types of damage. Isaacson (1977) has reviewed damage mechanisms that have been observed in the electron microscope and Pantano and Madey (1981) have summarized damage mechanisms that are manifested in AES. The details of the damage mechanism (dissociation, desorption, reduction, polymerization, oxidation, carburization, diffusion, etc.) are not sufficiently documented to predict damage rates in a variety of materials. It seems intuitively clear, however, that damage is related to energy transfer between the incident electron beam and the solid and thus to the magnitude of the inelastic scattering cross section. While not every inelastic scattering event will necessarily lead to specimen damage, the potential exists, in general, that the interactions which give rise to desired signals or properties may also lead to damage. The problem then is to identify the significant damage mechanisms in different types of material and to optimize the experimental conditions wherever possible to optimize the desired-signal/damage-rate ratio.

One important form of specimen damage is molecular dissociation. Dissociation of gas-phase molecules can be induced by direct electron bombardment. For solids, dissociation can be caused to a greater extent by the large number of low-energy secondary electrons which result from the decay of electronic excitations produced by primary electrons and other electrons in the collision cascade. The electronic excitations considered important are those of the valence electrons. For these excitations, the energy-loss function is large (Figs. 1-3) for $E \lesssim 50$ eV and the secondary electrons resulting from the decay of the excitation have energies for which the dissociation cross section is near its maximum value.

It has been recently discovered that molecular dissociation in some materials can be induced by another process. Inner-shell ionization of the cation of an ionic compound can decay most probably by inter-atomic Auger processes [Knotek and Feibelman (1978)] that can lead to a positively charged anion with a resulting "Coulomb explosion" of the molecule. The damage rate in such cases would then depend on the cross section for ionization of the particular cation inner-shell level. Whether damage in a given material was primarily associated with the excitation of valence electrons or the ionization of inner-shell levels could be determined from the dependence of the damage rate on electron (or photon) energy.

The concept of Auger-induced damage has been extended further by Ramaker *et al.* (1981) and Jennison *et al.* (1981). The ionization of inner-shell electrons in either ionic or covalent compounds can lead to decay by a core-valence-valence Auger process. If the two holes of the final state are localized in the vicinity of a bond sufficiently long, bond rupture may occur by a Coulomb explosion. If, on the other hand, the two holes are delocalized, damage will not occur. The extent of hole localization can be deduced from analysis of the resulting Auger-electron spectrum and damage rates in different compounds can be estimated [Ramaker *et al.* (1981)]. For materials in which Auger-induced damage is important, the damage rate should be proportional to a particular inner-shell ionization cross section.

5. SUMMARY

The basic theory for the inelastic scattering of electrons by atoms that was developed by Bethe and extended to solids appears generally satisfactory. Inelastic electron scattering by solids can be described by the so-called energy loss function derived from the complex frequency-dependent and momentum-dependent dielectric constant. There is still uncertainty, however, about the values of the parameters to use in the cross-section formulas, particularly in the parameter related to the momentum dependence of the energy-loss function. The extent to which the parameters may vary with atomic number and with electronic shell or subshell has not been adequately explored. Finally, there is uncertainty about the minimum electron energy for which the cross-section equations can be used with confidence.

Dielectric data (optical constants, the energy loss function) is available for a limited number of materials although often for a restricted range of frequencies or excitation energies. More dielectric data is required for use in cross-section formulas. Data is also needed to define significant physical processes in more detail, particularly the shape of the energy-loss function in the vicinity of inner-shell thresholds and the dependence of the energy-loss function on momentum transfer. Comparisons are needed of calculated generalized oscillator strengths and experimental data.

Presently available theory and experimental dielectric data provide a qualitative and in some cases quantitative guide to inelastic scattering cross sections appropriate for microanalysis (EELS), inner-shell ionization (EPMA, AES), surface analysis (AES, XPS), and radiation damage by electron bombardment. Improved understanding of inelastic-electron interactions and a larger data base should lead in the future to more accurate measurements or improved experimental designs.

Acknowledgement

The author wishes to thank Dr. C. Kunz for supplying Figs. 1-6. This work was supported in part by the Office of Environment, U.S. Department of Energy.

REFERENCES

Ashley JC and Tung CJ. (1982). Electron inelastic mean free paths in several solids for 200 eV $\leq$ E $\leq$ 10 keV. Surface and Interface Anal. **4**, 52-55.

Bambynek W, Crasemann B, Fink RW, Freund H-V, Mark, H, Swift CD, Price RE and Rao PV. (1972). X-ray fluorescence yields, Auger, and Coster-Kronig transition probabilities. Rev. Mod. Phys. **44**, 716-813.

Bethe H. (1930). Theory of passage of swift corpuscular rays through matter. Ann. der Physik. **5**, 325-400.

Citrin PH, Wertheim GK and Schlüter M. (1979). One-electron and many-body effects in x-ray absorption and emission edges of Li, Na, Mg, and Al metals. Phys. Rev. B **20**, 3067-3114.

Dietz RE, McRae EG and Weaver JH. (1980). Core-electron excitation edges in metallic Ni, Cu, Pt, and Au. Phys. Rev. B **21**, 2229-2247.

Drawin H-W. (1963). Zur spektroskopischen Temperatur und Dichtemessung von Plasmen bei Abwesenheit Thermodynamischen Gleichgewichtes. (Spectroscopic temperature and density measurement of plasmas in the absence of thermodynamic equilibrium.) Z. Phys. **172**, 429-452.

Fano U and Cooper JW. (1968). Spectral distribution of atomic oscillator strengths. Rev. Mod. Phys. **40**, 441-507.

Fischer B and Hoffman K-W. (1967). Die intensität der bremsstrahlung und der charakteristischen K-Röntgenstrahlung dünner anoden. (The intensities of bremsstrahlung and characteristic K x-rays of thin anodes.) Z. Physik. **204**, 122-128.

Gadzuk JW. (1978). Many-body effects in Photemission. In: Photoemission and the Electron Properties of Surfaces, B. Feuerbacher, B. Fitton, and R.F. Willis (eds.), Wiley, New York, 111-136.

Green M and Cosslett VE. (1961). The efficiency of production of characteristic x-radiation in thick targets of a pure element. Proc. Phys. Soc. (London) **78**, 1206-1214.

Gryzinski M. (1965). Classical theory of atomic collisions. I. Theory of inelastic collisions. Phys. Rev. **138**, A336-A358.

Haelbich R-P, Iwan M and Koch EE. (1977). Optical properties of some insulators in the vacuum ultraviolet region. Physik Daten-Physics Data (Zentralstelle für Atomkernenergie-Dokumentation, Eggenstein-Leopoldshafen), 1-186.

Hagemann H-J, Gudat W and Kunz C. (1974). Optical constants from the far infrared to the x-ray region: Mg, Al, Cu, Ag, Au, Bi, C, and Al_2O_3. Deutsches Elektronen-Synchrotron Report SR-74/7 (Hamburg).

Inokuti M. (1971). Inelastic collisions of fast charged particles with atoms and molecules—the Bethe theory revisited. Rev. Mod. Phys. **43**, 297-347.

Inokuti M and Manson ST. (1983). Cross-sections for inelastic scattering of electrons by atoms—selected topics related to electron microscopy, In: Electron Beam Interactions, SEM, Inc., AMF O'Hare, IL (this volume), 1-17.

Isaacson M. (1977). Specimen damage in the electron microscope, In: Principles and Techniques of Electron Microscopy, M.A. Hayat (ed.), Van Nostrand-Reinhold, New York, Vol. 7, 1-78.

Jach TJ and Powell CJ. (1981). Incident-energy dependence of 3p electron energy-loss spectra of nickel. Sol. State Comm. **40**, 967-969.

Jennison DR, Kelber JA and Rye RR. (1981). Localized Auger final states in covalent systems. J. Vac. Sci Tech. **18**, 466-467.

Knotek ML and Feibelman PJ. (1978). Ion desorption by core-hole Auger decay. Phys. Rev. Lett. **40**, 964-967.

Kolbenstvedt H. (1967). Simple theory for K-ionization by relativistic electrons. J. Appl. Phys. **38**, 4785-4787.

Leapman RD and Grunes LA. (1980). Anomalous L_3/L_2 white-line ratios in the 3d transition metals. Phys. Rev. Lett. **45**, 397-401.

Leapman RD, Rez P and Mayers DF. (1980). K, L, and M shell generalized oscillator strengths and ionization cross sections for fast electron collisions. J. Chem. Phys. **72**, 1232-1243.

Lotz W. (1970). Electron impact ionization cross sections for atoms. Z. Phys. **232**, 101-107.

McGuire EJ. (1971). Inelastic scattering of electrons and protons by the elements He to Na. Phys. Rev. A **3**, 267-279.

Mott NF and Massey HSW. (1949). The theory of atomic collisions, Oxford University Press, London (second edition), 243-244.

Pantano CG and Madey TE (1981). Electron beam damage in Auger electron spectroscopy. Appl. Surf. Sci. **7**, 115-141.

Penn DR. (1976). Quantitative chemical analysis by ESCA. J. Elect. Spect. **9**, 29-40.

Powell CJ. (1969). Analysis of optical- and inelastic-electron-scattering data. Parametric calculations. J. Opt. Soc. Am. **59**, 738-743.

Powell CJ. (1974). Attenuation lengths of low-energy electrons in solids. Surf. Sci. **44**, 29-46.

Powell CJ. (1976a). Cross sections for ionization of inner-shell electrons by electrons. Rev. Mod. Phys. **48**, 33-47.

Powell CJ. (1976b). Evaluation of formulas for inner-shell ionization cross sections, In: Proceedings of a Workshop on the Use of Monte Carlo Calculations in Electron Probe Microanalysis and Scanning Electron Microscopy, K.F.J. Heinrich, D.E. Newbury, and H. Yakowitz (eds.), U.S. National Bureau of Standards Special Publication 460, Washington, 97-104.

Powell CJ. (1978). The physical basis for quantitative surface analysis by Auger electron spectroscopy and x-ray photoelectron spectroscopy, In: Quantitative Surface Analysis of Materials, N.S. McIntyre (ed.), American Society for Testing and Materials Special Technical Publication 634, Philadelphia, 5-29.

Raether H. (1980). Excitation of plasmons and interband transitions in solids. Springer Tracts in Modern Physics 88, Springer-Verlag, New York, 1-196.

Ramaker DE, White CT and Murday JS. (1981). Auger-induced desorption of covalent and ionic systems. J. Vac. Sci. Tech. **18**, 748-749.

Rudge MRH and Schwartz SB. (1966). The ionization of hydrogen and of hydrogenic positive ions by electron impact. Proc. Phys. Soc. (London) **88**, 563-578.

Schnatterly SE. (1979). Inelastic scattering spectroscopy, In: Solid State Physics, H. Ehrenreich, F. Seitz and D. Turnbull (eds.), Academic Press, New York, Vol. 34, 275-358.

Seah MP and Dench WA. (1979). Quantitative electron spectroscopy of surfaces: A standard data base for electron mean free paths in solids. Surf. Interface Anal. **1**, 2-11.

Shiles E, Sasaki T, Inokuti M and Smith DY. (1980). Self-consistency and sum-rule tests in the Kramers-Kronig analysis of optical data: Applications to aluminum. Phys. Rev. B **22**, 1612-1628.

Shirley DA. (1978). Many-electron and final-state effects: Beyond the one-electron picture, In: Photoemission in Solids I, M. Cardona and L. Ley (eds.), Springer Topics in Applied Physics 26, Springer-Verlag, New York, 165-195.

Siegbahn K, Allison DA and Allison JH. (1974). ESCA-photoelectron spectroscopy, In: Handbook of Spectroscopy, CRC Press, Cleveland, Vol. 1, 257-752.

Smith DM and Gallon TE. (1974). Auger emission from solids: The estimation of backscattering effects and ionization cross sections. J. Phys. D **7**, 151-161.

Swanson N and Powell CJ. (1968). Excitation of L-shell electrons in Al and Al_2O_3 by 20 keV electrons. Phys. Rev. **167**, 592-600.

Szajman J and Leckey RCG. (1981). An analytical expression for the calculation of electron mean free paths in solids. J. Elect. Spect. **23**, 83-96.

Szajman J, Liesegang J, Jenkin JG and Leckey RCG. (1981). Is there a universal mean-free-path curve for electron inelastic scattering in solids? J. Elect. Spect. **23**, 97-102.

Teo BK and Joy DC. (eds.) (1981). EXAFS spectroscopy, techniques and applications, Plenum Press, New York, 1-272.

Wagner CD, Riggs WM, Davis LE, Moulder JF and Muilenberg GE. (1979). Handbook of x-ray photoelectron spectroscopy, Perkin Elmer-Physical Electronics Division, Eden Prairie, Minn.

Wagner CD, Davis LE and Riggs WM. (1980). The energy dependence of the electron mean free path. Surf. Interface Anal. **2**, 53-55.

Weaver JH, Krafka C, Lynch DW and Koch EE. (1981). Optical properties of metals. Physik Daten-Physics Data (Fachinformations-zentrum, Karlsruhe, W. Germany), 1-302.

Winick H and Doniach S. (eds.) (1980). Synchroton Radiation Research, Plenum Press, New York, 1-754.

Worthington CR and Tomlin SG. (1956). The intensity of emission of characteristic x-radiation. Proc. Phys. Soc. (London) A **69**, 401-412.